Control of the Redox Potential of *Pseudomonas aeruginosa* Cytochrome c_{551} through the Fe−Met Coordination Bond Strength and pK_a of a Buried Heme Propionic Acid Side Chain†

Shin-ichi J. Takayama,‡ Shin-ichi Mikami,‡ Norifumi Terui,‡ Hajime Mita,‡ Jun Hasegawa,§ Yoshihiro Sambongi,|| and Yasuhiko Yamamoto*,‡

Department of Chemistry, University of Tsukuba, Tsukuba 305-8571, Japan, Daiichi Pharmaceutical Company, Ltd., Edogawa-ku, Tokyo 134-8630, Japan, and Graduate School of Biosphere Science, Hiroshima University, Higashi-Hiroshima 739-8528, Japan

Received November 29, 2004; Revised Manuscript Received February 22, 2005

ABSTRACT: *Pseudomonas aeruginosa* cytochrome c_{551} and a series of its mutants exhibiting various thermostabilities have been studied by paramagnetic ^{1}H NMR and cyclic voltammetry in an effort to elucidate the molecular mechanisms responsible for control of the redox potentials ($E^{\circ\prime}$) of the proteins. The study revealed that the $E^{\circ\prime}$ value of the protein is regulated by two molecular mechanisms operating independently of each other. One is based on the Fe−Met coordination bond strength in the protein, which is determined by the amino acid side chain packing in the protein, and the other on the pK_a of the heme 17-propionic acid side chain, which is affected by the electrostatic environment. The former mechanism alters the magnitude of the $E^{\circ\prime}$ value throughout the entire pH range, and the latter regulates the pK values reflected by the pH profile of the $E^{\circ\prime}$ value. These findings provide novel insights into functional regulation of the protein, which could be utilized for tuning the $E^{\circ\prime}$ value of the protein by means of protein engineering.

Understanding the molecular mechanisms responsible for control of the redox potentials ($E^{\circ\prime}$)[1] of proteins is fundamentally and practically important. Such understanding should lead to a quantitative description of the way proteins control the specificity and efficiency of key biological processes. The proper way of accomplishing this important task has remained an open question even after the thorough elucidation of the X-ray structures of redox active proteins (*1*−*5*). Monoheme class I cytochromes *c* (cyts *c*), in which the heme Fe is coordinated to the His $N^{\delta 2}$ and Met S^{δ} atoms as axial ligands at the redox center, are some of the best characterized redox active proteins (*6*, *7*). Homologous *Pseudomonas aeruginosa* cytochrome c_{551} (PA) (*8*) and *Hydrogenobacter thermophilus* cytochrome c_{552} (HT) (*9*) exhibit 56% sequence homology with each other and hence exhibit almost identical protein folding (*10*, *11*). Despite their structural similarity, there is remarkable disparity in their thermostability and redox properties; the denaturation temperature (T_m) of PA is considerably lower than that of HT, and the $E^{\circ\prime}$ value of PA at pH 5.0 and 25 °C is higher by ∼80 mV than that of HT (Table 1) (*12*−*15*). To understand the differences between these homologous proteins, site-directed mutants of PA, for which amino acid substitutions were selected with reference to the corresponding residues in HT, have been prepared and subjected to a detailed study on their structure−function relationship (*11*−*16*). The study demonstrated that the overall protein stabilities and redox functions of the cyts *c* are interrelated with each other through the stability of the Fe−S bond (*15*, *16*).

In general, the Gibbs energy change for the reduction of the oxidized form of a redox active protein (ΔG_{redox}) is described as four major terms (*17*, *18*)

$$\Delta G_{redox} = \Delta G_{RC} + \Delta G_{EI} + \Delta G_{CC} + \Delta G_{L} \qquad (1)$$

where ΔG_{RC} is the Gibbs energy difference between the oxidized and reduced states resulting from bonding interactions at the redox center, ΔG_{EI} is the Gibbs energy difference resulting from electrostatic interactions between the redox center charge and polar groups within both the protein and the solvent, ΔG_{CC} arises from Gibbs energy changes that can be attributed to redox-dependent conformation changes of the protein, and ΔG_{L} arises from differential binding of ligands to the oxidized and reduced forms of the protein.

We have recently demonstrated in the studies on PA and HT as well as a series of PA mutants that the $E^{\circ\prime}$ value of the protein is regulated through the Fe−S bond stability in the oxidized protein (*15*). This $E^{\circ\prime}$ regulation can be simply interpreted in terms of the ΔG_{RC} contribution. The Fe−S

† This work was supported by a research grant (15550143) from the Ministry of Education, Science, Sports, Culture, and Technology. This work was also supported by a University of Tsukuba Research Project (A).

* To whom correspondence should be addressed. Phone and fax: +81-29-853-6521. E-mail: yamamoto@chem.tsukuba.ac.jp.

‡ University of Tsukuba.

§ Daiichi Pharmaceutical Company, Ltd.

|| Hiroshima University.

[1] Abbreviations: $E^{\circ\prime}$, redox potential; cyt *c*, cytochrome *c*; PA, *P. aeruginosa* cytochrome c_{551}; HT, *H. thermophilus* cytochrome c_{552}; T_m, denaturation temperature; qm, F7A/V13M/F34Y/E43Y/V78I quintuple mutant; CV, cyclic voltammetry; δ−pH plots, plots of observed shifts of heme methyl proton signals of proteins against pH; $E^{\circ\prime}$−pH plots, plots of redox potentials of proteins against pH.

10.1021/bi047498s CCC: $30.25
Published on Web 03/18/2005

Table 1: pK_a Values, $E^{\circ\prime}$ Values, and Denaturation Temperatures of PA, PA Mutants, and HT

	NMR	CV		$E^{\circ\prime}$ [c]	T_m [d]	T_{Fe-S} [e]
	pK_a [a]	pK_{ox} [b]	pK_{red} [b]	(mV)	(°C)	(°C)
PA	6.1	5.9	7.0	321	50.4	78
E43Y	5.0	5.0	6.0	309	55.5	82
F34Y	<4.5	<4.5	<5.5	274	66.4	89
F7A/V13M/V78I	6.2	6.0	7.0	248	68.4	90
F34Y/E43Y	<4	<4	<5	277	70.7	90
F7A/V13M/F34Y/E43Y/V78I (qm)	<4	<4	<5	214	83.9	>100
HT	<4	<4	<5	245	91.8	>100

[a] The value was obtained from the pH-dependent shifts of the heme methyl proton signals of the oxidized form of the protein. The experimental error was ±0.2. [b] pK_{ox} and pK_{red} represent the pK_a values of the oxidized and reduced forms of the protein, respectively, determined on fitting of the pH profile of the $E^{\circ\prime}$ value to the Nernst equation (see the Supporting Information). The experimental error was ±0.2. [c] Determined at pH 5.0 and 25 °C. The experimental error determined from the deviation of two or more experiments was ±5 mV. [d] The denaturation temperature of the oxidized protein at pH 5.0 and in the presence of 1.5 M guanidine hydrochloride (*11*, *12*). [e] The dissociation of the Fe−S coordination bond of the oxidized protein at pH 7.0, determined from the temperature dependence of the 695 nm absorption band characteristic of the bond (see the Supporting Information).

bond stability of the protein is determined by the amino acid side chain packing, which is affected by the protein conformation change induced by the mutations (*16*). Furthermore, it has been shown that the overall protein stability, and hence the Fe−S bond stability, of the reduced form is less affected by mutations than that of the oxidized one (*19*). Generally, cationic ferriheme in the oxidized protein is less favorable in the hydrophobic environment of the heme pocket compared with neutral ferroheme in the reduced one (*20*−*25*). In a protein with higher stability, the ferriheme is stabilized through a stronger Fe−S bond, leading to regulation of the redox properties of the proteins. As a result, the $E^{\circ\prime}$ value of a mutant with a higher stability exhibits a more negative shift relative to that of wild-type PA in an enthalpic manner (*15*). On the other hand, ΔG_{EI} is due to the point charges of acidic and basic residues, the partial charges of all protein atoms, and solvation effects, and has been shown to play a significant role in determining ΔG_{redox} (*17*, *18*, *26*). In the case of cyts *c*, the influence of the ionization state of the heme propionic acid side chain on the $E^{\circ\prime}$ value has attracted considerable attention (*27*−*33*). In particular, the pK_a values reflected by the pH profiles of the midpoint oxidation−reduction potentials of various cyts *c* have been attributed predominantly to ionization of the heme 17-propionic acid side chain (*28*). Furthermore, the redox-dependent structure change in horse cyt *c* has been analyzed in detail to identify the structure factors responsible for the ΔG_{CC} contribution (*34*−*37*). The magnitude of the ΔG_{CC} contribution and its structural origin remain to be explored. Finally, the ΔG_L contribution can be neglected upon analysis of the $E^{\circ\prime}$ value of cyt *c*.

In our study, we have extended our paramagnetic ^{1}H NMR and electrochemical studies on a series of PA mutants, i.e., the F34Y single, E43Y single, F34Y/E43Y double, F7A/V13M/V78I triple, and F7A/V13M/F34Y/E43Y/V78I quintuple (qm) mutants (Figure 1), to determine the molecular mechanism responsible for the $E^{\circ\prime}$ regulation of the proteins. A study on these proteins provides a unique opportunity for

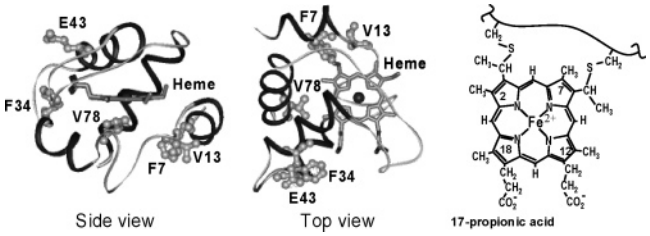

FIGURE 1: Schematic representation (side and top views) of the structure of *P. aeruginosa* cytochrome c_{551} (PA), and the locations of amino acid residues substituted in the F7A/V13M/F34Y/E43Y/V78I quintuple mutant (qm). The polypeptide chain is illustrated as a ribbon model, and the heme is drawn as a stick model. The five substituted residues are shown as a ball-and-stick model. The molecular structure and numbering system for the heme are given at the right.

detailed characterization of the effects of the Fe−S bond stability as well as the ionization of the heme 17-propionic acid side chain on the $E^{\circ\prime}$ value. As summarized in Table 1, they exhibit various thermostabilities in the protein structure as well as the Fe−S bond between those of PA and HT, and the effects of the individual mutations on the protein structure have been fully characterized (*11*−*13*). Furthermore, since both F34 and E43 in PA are adjacent to the heme 17-propionic acid side chain (*8*), the ionization of the heme 17-propionic acid side chain in the protein is expected to be affected by mutations of these residues. The ^{1}H NMR spectra and $E^{\circ\prime}$ values of the proteins over a wide pH range have been characterized to determine the molecular mechanisms responsible for control of the $E^{\circ\prime}$ value. The $E^{\circ\prime}$ values of cyts *c* were found to be regulated through the Fe−S bond stability and the ionization state of the heme 17-propionic acid side chain.

MATERIALS AND METHODS

Protein Samples. Wild-type PA and the mutants were produced using *Escherichia coli* and purified as reported previously (*11*, *12*). The oxidized forms of the proteins were prepared by the addition of a 10-fold molar excess of potassium ferricyanide. For NMR samples, the proteins were concentrated to ~1 mM in an ultrafiltration cell (YM-5, Amicon), and then 10% ^2H_2O was added to the protein solutions. The pH of each sample was adjusted using 0.2 M KOH or 0.2 M HCl, and the pH was monitored with a Horiba F-22 pH meter with a Horiba type 6069-10C electrode.

Cyclic Voltammetry. The procedures used for obtaining cyclic voltammograms of the proteins were essentially the same as those described previously (*15*, *38*−*40*). Cyclic voltammetry (CV) experiments were performed with a PGSTAT12 potentiostat-galvanostat (Autolab). A gold electrode treated with 4,4′-dipyridyl disulfide just before use was employed as the working electrode. An Ag|AgCl electrode in a saturated NaCl solution and a Pt wire were employed as the reference and counter electrodes, respectively. The potential sweep range was from +350 to −150 mV versus the Ag|AgCl electrode in a saturated NaCl solution with a scan rate of 20 mV s^{-1}. All potentials are referenced to the standard hydrogen electrode. The protein concentration was ~0.5 mM in 20 mM phosphate buffer (pH 4.0−9.0) and 0.1 M $NaClO_4$. All experiments were performed at 25 °C under a nitrogen atmosphere. The anodic to cathodic peak current ratios obtained at various potential scan rates (1−100 mV

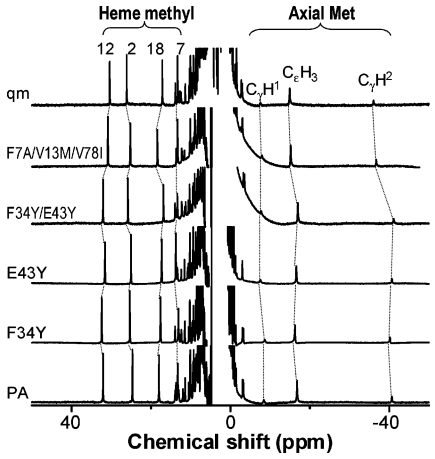

FIGURE 2: ^{1}H NMR spectra (600 MHz) of the oxidized forms of PA and the F34Y single, E43Y single, F34Y/E43Y double, F7A/V13M/V78I triple, and F7A/V13M/F34Y/E43Y/V78I quintuple (qm) mutants in a 90% H_2O/10% ^2H_2O mixture at pH 7.0 and 25 °C. The heme methyl and axial Met side chain proton resonances are given with the spectra, and the corresponding resonances are connected by dotted lines.

s^{-1}) were all ~1. Both the anodic and cathodic peak currents increased linearly as a function of the square root of the scan rate in the range up to 100 mV s^{-1}. The anodic and cathodic peak separations of the scan rate in the range up to 100 mV s^{-1} were approximately 100 mV. Thus, PA and its mutants exhibit quasi-reversible redox processes.

^{1}H NMR. NMR spectra were recorded on a Bruker Avance 600 FT NMR spectrometer operating at a ^{1}H frequency of 600 MHz. Chemical shifts are given in parts per million downfield from sodium 2,2-dimethyl-2-silapentane-5-sulfonate with H_2O as an internal reference.

Absorption Spectroscopy. Absorption spectra at 695 nm were recorded with a Beckman DU 640 spectrophotometer using a micro T_m analysis system and a micro T_m cell. The protein concentration was ~0.2 mM in 20 mM phosphate buffer (pH 7.0) in the presence of 10 mM potassium ferricyanide.

RESULTS

^{1}H NMR Spectra of PA and Its Mutants, and Their pH Profiles. We first analyzed the effects of amino acid substitutions on the heme electronic structure of the protein by paramagnetic ^{1}H NMR measurement. The 600 MHz ^{1}H NMR spectra of the oxidized forms of PA and the mutants are compared with each other in Figure 2. The heme electronic structures in the proteins have been shown to be sensitively manifested in paramagnetic shifts of the heme peripheral side chain proton signals of the oxidized proteins (*41*−*43*). The spectral patterns observed for all the proteins were essentially similar to each other, indicating that the structural properties of the heme active site were not significantly affected by the amino acid substitution(s) introduced into the mutants.

Spectra of the proteins at various pHs were recorded (see the Supporting Information), and the observed shifts of the heme methyl proton signals of the proteins, PA, and the F34Y single, E43Y single, F34Y/E43Y double, F7A/V13M/V78I triple, and F7A/V13M/F34Y/E43Y/V78I quintuple (qm) mutants, are plotted against pH (δ−pH plots) in Figure 3. The δ−pH plots of PA were essentially identical to those reported previously and reflected the pK_a value of 6.1 ± 0.2, which can be attributed to ionization of the heme 17-propionic acid side chain (*28*, *32*). A similar pK_a value was also determined from the δ−pH plots for the F7A/V13M/V78I triple mutant. Furthermore, the pK_a value of 5.0 ± 0.2 was determined from the δ−pH plots for the E43Y single mutant. pK_a values at least 2 pH units lower than that of PA were determined for the F34Y single mutant, the F34Y/E43Y double mutant, and qm. These results demonstrated that the pK_a value of the heme 17-propionic acid side chain in PA is affected by the F34Y and E43Y mutations.

pH Profile of the $E^{\circ\prime}$ Value of PA. We next measured $E^{\circ\prime}$ values of PA at various pHs, and the obtained values are plotted against pH ($E^{\circ\prime}$−pH plots) in Figure 4A. As shown in the $E^{\circ\prime}$−pH plots, the $E^{\circ\prime}$ value of PA was ~260 mV at pH 8.0 and exhibited a positive shift of ~60 mV with a decrease in pH to 4.5. The fitting of the plots to the Nernst equation (*44*) yielded pK values of 5.9 ± 0.2 and 7.0 ± 0.2 for the oxidized and reduced forms (pK_{ox} and pK_{red}), respectively (see the Supporting Information). The value obtained for the oxidized form was essentially equal to the pK_a value, 6.1 ± 0.2, of the heme 17-propionic acid side chain determined from the δ−pH plots in Figure 3 (*28*, *32*). This confirmed that the $E^{\circ\prime}$ value of the protein is affected by ionization of the heme 17-propionic acid side chain.

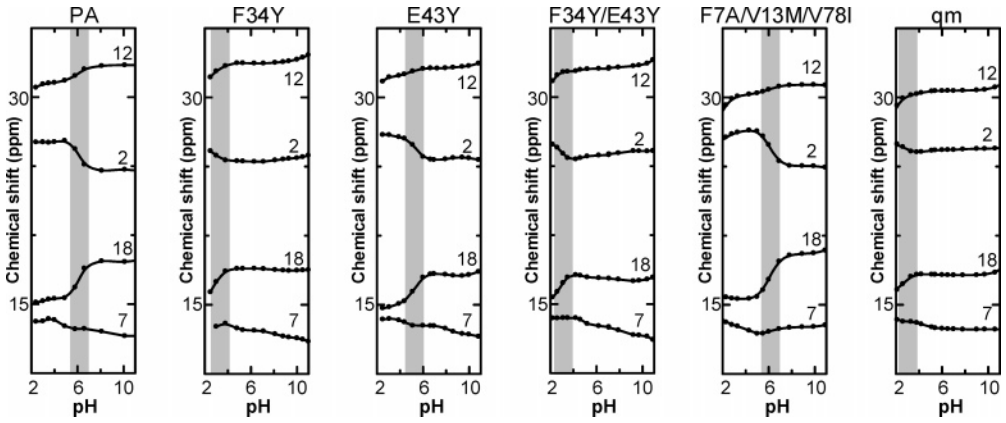

FIGURE 3: pH dependence of the chemical shifts of the heme methyl proton signals of the oxidized forms of PA and the F34Y single, E43Y single, F34Y/E43Y double, F7A/V13M/V78I triple, and F7A/V13M/F34Y/E43Y/V78I quintuple (qm) mutants in a 90% H_2O/10% ^2H_2O mixture at 25 °C. The pH region in which the heme methyl proton signals exhibited large pH-dependent shifts is shaded gray.

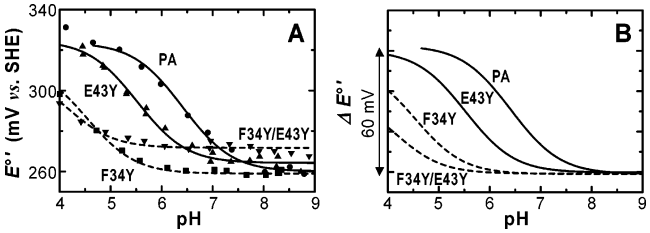

FIGURE 4: (A) Plots of the redox potentials ($E^{\circ\prime}$) against pH for PA and the F34Y single, E43Y single, and F34Y/E43Y double mutants at 25 °C. The solid curves for PA and the E43Y single mutant are theoretical curves drawn using the pH-dependent form of the Nernst equation, $E^{\circ\prime} = E_H^{\circ\prime} - 0.06 \log[(K_{ox} + [H^+])/(K_{red} + [H^+])]$, where $E_H^{\circ\prime}$ is the $E^{\circ\prime}$ of the fully protonated form and K_{ox} and K_{red} are the equilibrium constants for the ionization in the oxidized and reduced proteins, respectively (*44*). The dashed lines for the F34Y single and F34Y/E43Y double mutants do not represent theoretical curves but schematic representations of the patterns of their $E^{\circ\prime}$−pH plots. (B) Fitting of the plots for PA and the E43Y single mutant in panel A to the Nernst equation, the patterns of the plots for the F34Y single and F34Y/E43Y double mutants being replotted in such a way that the $E^{\circ\prime}$ values of all the proteins at pH 9.0 equaled a constant value, i.e., $\Delta E^{\circ\prime}$ ($=E_i^{\circ\prime} - E_{9.0}^{\circ\prime}$, where $E_i^{\circ\prime}$ and $E_{9.0}^{\circ\prime}$ represent the $E^{\circ\prime}$ values at pH i and 9.0, respectively), to compare the pK_a values determined from the pH profiles of the $E^{\circ\prime}$ values.

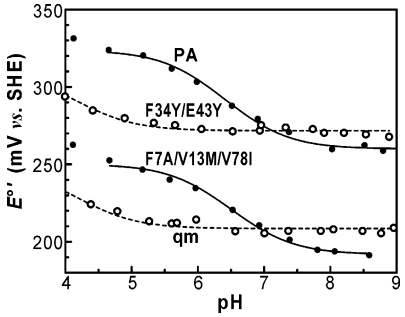

FIGURE 5: Plots of the redox potentials ($E^{\circ\prime}$) against pH for PA and the F34Y/E43Y double, F7A/V13M/V78I triple, and F7A/V13M/F34Y/E43Y/V78I quintuple (qm) mutants. The $E^{\circ\prime}$−pH plots for PA are essentially parallel to those for the F7A/V13M/V78I triple mutant, with a difference in magnitude of the $E^{\circ\prime}$ value of ~70 mV. Fitting of the plots to the Nernst equation yielded pK_a values of 5.9 ± 0.2 and 7.0 ± 0.2 for the oxidized and reduced forms of PA, respectively, and values of 6.0 ± 0.2 and 7.0 ± 0.2 for the oxidized and reduced forms of the F7A/V13M/V78I triple mutant, respectively (see the Supporting Information). The patterns of the $E^{\circ\prime}$−pH plots for the F34Y/E43Y double mutant and qm are similar to each other, with a difference in magnitude in the $E^{\circ\prime}$ value of ~70 mV. The pK_a values for the F34Y/E43Y double mutant and qm were too low to be determined from the fitting.

According to the X-ray structure of PA (*8*), the heme 17-propionic acid side chain is buried in the protein matrix, and is proposed to be hydrogen-bonded to the side chains of R47 and W56, while the heme 13-propionic acid side chain is largely exposed to the solvent, exhibiting a pK_a value of ~3.5 (*27*). In the $E^{\circ\prime}$−pH plots, the $E^{\circ\prime}$ value exhibited a positive shift with a further decrease in pH to <4.5, which could be attributed to protonation of the heme 13-propionate side chain. The δ−pH plots of PA in Figure 3 also revealed a pH-dependent change below pH 4.0.

pH Profiles of the E°′ Values of the F34Y Single, E43Y Single, and F34Y/E43Y Double Mutants. The $E^{\circ\prime}$−pH plots for the F34Y single, E43Y single, and F34Y/E43Y double mutants were similarly characterized and are compared with those for PA in Figure 4A. Fitting of the plots to the Nernst equation yielded values of 5.0 ± 0.2 and 6.0 ± 0.2 for pK_{ox} and pK_{red} of the E43Y single mutant, respectively (see the Supporting Information). The values of the F34Y single mutant were too low to be determined quantitatively from the fitting, <4.5 and <5.5 being estimated for pK_{ox} and pK_{red}, respectively. Furthermore, the pK_{ox} and pK_{red} values of the F34Y/E43Y double mutant were lower by at least 2 pH units relative to those of PA. The similar pK_{ox} values of the proteins were also manifested in the δ−pH plots of the corresponding proteins illustrated in Figure 3. To highlight the differences in the pK value, manifested in the $E^{\circ\prime}$−pH plots, among the proteins, the data were plotted in such a way that the $E^{\circ\prime}$ values of all the proteins at pH 9.0 equaled a constant value (Figure 4B).

On the basis of the $E^{\circ\prime}$−pH plots, the proteins could be ranked in order of increasing pK value: F34Y/E43Y < F34Y < E43Y < PA. Comparison of the pK_a values of the heme 17-propionic acid side chain among the F34Y single, E43Y single, and F34Y/E43Y double mutants showed that the effect of the F34Y mutation on the pK_a value is larger than that of the E43Y mutation, and that the F34Y and E43Y mutations alter the pK_a value in an almost additive manner (Figure 4B).

pH Profile of the E°′ Value of the F7A/V13M/V78I Triple Mutant. The effect of F7A, V13M, and V78I amino acid substitutions in the triple mutant on the $E^{\circ\prime}$ value was examined (Figure 5). Comparison of the $E^{\circ\prime}$−pH and δ−pH plots between PA and the F7A/V13M/V78I triple mutant showed that their $E^{\circ\prime}$−pH plots were quite similar in pattern to each other, the exception being the difference of ~70 mV in magnitude throughout the pH range that was examined. The fitting of the $E^{\circ\prime}$−pH plots to the Nernst equation yielded pK_{ox} and pK_{red} values of 6.0 ± 0.2 and 7.0 ± 0.2 for the F7A/V13M/V78I triple mutant, respectively (see the Supporting Information), and the pK_a value of the heme 17-propionic acid side chain was determined to be 6.2 ± 0.2 from its δ−pH plots in Figure 3. The similarity in the pK_a values between PA and the F7A/V13M/V78I triple mutant demonstrated that the ionization of the heme 17-propionic acid side chain was not affected by the F7A, V13M, and V78I mutations.

pH Profiles of the E°′ Value of qm. The $E^{\circ\prime}$−pH plots for qm were characterized, and are compared with those of PA, the F34Y/E43Y double mutant, and the F7A/V13M/V78I triple mutant in Figure 5. Similar to the relationship between the $E^{\circ\prime}$−pH plots for PA and the F7A/V13M/V78I triple mutant, those for the F34Y/E43Y double mutant and qm were similar in pattern to each other with a difference of ~70 mV in magnitude throughout the pH range that was examined. In the $E^{\circ\prime}$−pH plots for the F34Y/E43Y double mutant and qm, a pH-dependent change in the $E^{\circ\prime}$ value was observed below pH 5, indicating that the pK_{ox} and pK_{red} values of the F34Y/E43Y double mutant and qm were lower by at least 2 pH units than those of PA and the F7A/V13M/V78I triple mutant. The considerable decreases in the pK_{ox} and pK_{red} values of the F34Y/E43Y double mutant and qm essentially paralleled the dramatic decrease in the pK_a value of the heme 17-propionic acid side chain, as shown in their δ−pH plots in Figure 3. Comparison of the pK_a values among the F34Y/E43Y double mutant, the F7A/V13M/V78I triple mutant, and qm strongly suggested that the F34 and E43 residues are crucial in determining the pK_a value of the

heme 17-propionic acid side chain, and hence in regulation of the pK value of the pH profile of the $E^{\circ\prime}$ value for the protein through the ΔG_{EI} contribution.

DISCUSSION

Heme Active Site Structures in the Proteins. As shown in the NMR spectra in Figure 2, most signals for the mutants were observed in the shift range between the corresponding signals for the wild-type PA and qm. The NMR solution structure of qm has been shown to be highly similar to the X-ray crystal structure of PA (*12*). Additionally, the similarity in the heme coordination structure between the oxidized forms of PA and qm was also confirmed in the paramagnetic NMR study, which demonstrated that their paramagnetic susceptibility tensors determined upon analysis of the redox-dependent ^{1}H NMR shifts were essentially identical (*45*). Therefore, considering the structural similarity between the wild-type PA and qm, the heme active site structures in the other mutants were expected to be similar to each other. This conclusion was supported by other spectroscopic data (*13*, *14*).

Despite the structural similarity among the proteins, the pK_a value of the heme 17-propionic acid side chain of PA was influenced by the F34Y and E43Y mutations. The X-ray structure of PA indicated that F34 and E43 are located in the proximity of the heme 17-propionic acid side chain, which forms an ion pair with the guanidyl group of the R47 side chain and a hydrogen bond with the W56 side chain N_ϵH proton (*8*). The side chains of Tyr residues introduced by the F34Y and E43Y mutations into wild-type PA are likely to interact with the heme 17-propionic acid side chain in either a direct manner or an indirect one through the R47 or W56 side chain. Such an interaction could influence the electronic environment around the heme 17-propionic acid side chain and result in enhancement of the overall protein stability of PA (Table 1) (*11*, *13*). The two introduced Tyr aromatic side chains in qm have been suggested to interact with each other through a hydrophobic interaction (*11*). However, the additive effects of the F34Y and E43Y mutations on the pK_a value of the heme 17-propionic acid side chain, as demonstrated in Figure 4, strongly suggested the absence of a concerted action of these Tyr side chains upon the interaction with the heme 17-propionic acid side chain. The pK_a of a titrating group in proteins is sensitively affected by not only its electrostatic environment but also nonelectrostatic interactions. For example, the amount of water nearby, the extent of burial, and the flexibility of polar side chains around a titrating group all depend on a balance of interactions, including van der Waals and hydrophobic interactions (*46*). According to the X-ray structure of PA (*8*), the nearest water molecule is at least 0.47 nm from the carboxylic group of the buried heme 17-propionic acid side chain, whereas a single water molecule is hydrogen bonded to the exposed heme 13-propionic acid side chain. Hence, the effect of the water molecule on the pK_a value of the heme 17-propionic acid side chain would be only subtle. The molecular mechanism responsible for the decrease in the pK_a value of the buried heme 17-propionic acid side chain in the F34Y single, E43Y single, and F34Y/E43Y double mutants remains to be characterized.

pH Profile of the $E^{\circ\prime}$ Value. The $E^{\circ\prime}$ values of the proteins exhibited positive shifts with a decrease in pH, as shown in Figures 4 and 5. Since the $E^{\circ\prime}$ value of a protein is related to the difference in thermodynamic stability between the two redox forms, the negative shift of the $E^{\circ\prime}$ value with an increase in pH could be interpreted simply in terms of the stabilization of cationic ferriheme in the oxidized protein, relative to neutral ferroheme in the reduced one, in the hydrophobic environment of the heme active site through partial neutralization of its positive charge by the heme 17-propionate side chain (*28*, *32*). Thus, the differences in the pK value, manifested in the $E^{\circ\prime}$−pH plots, among the proteins can be attributed solely to the effects of the amino acid substitution(s) on the physicochemical environment around the buried heme 17-propionic acid side chain. In general, a charged group in a hydrophobic environment inside a protein is unstable and is stabilized through neutralization upon electrostatic interaction with nearby polar group(s). It has been proposed that the heme propionate side chain buried in the protein matrix of cyt *c* is hydrogen-bonded to the positively charged amino acid side chain of a Lys or Arg residue to lower its pK_a value to maintain a constant $E^{\circ\prime}$ value throughout the physiological pH range (*27*). As described above, the X-ray structure of PA demonstrated that the heme 17-propionate side chain forms an ion pair with the R47 side chain (*8*). However, the pK_a values of PA, i.e., 5.9 ± 0.2 and 7.0 ± 0.2, for the oxidized and reduced forms, respectively, obtained from the $E^{\circ\prime}$−pH plots indicated that the electrostatic interaction between the heme 17-propionate and R47 side chains is rather weak, if it exists. Therefore, the ranking of the proteins as qm (F7A/V13M/F34Y/E43Y/V78I) ≈ F34Y/E43Y < F34Y < E43Y < F7A/V13M/V78I ≈ PA, in order of increasing pK_a value, is likely to reflect the degree of stabilization of the deprotonated state of the heme 17-propionic acid side chain in the protein interior.

Molecular Mechanisms for Control of the $E^{\circ\prime}$ Value in PA. The $E^{\circ\prime}$−pH plots in Figures 4 and 5 clearly demonstrate that there are two mechanisms for the control of the $E^{\circ\prime}$ values of the proteins. One is a mechanism that alters the magnitude of the $E^{\circ\prime}$ value throughout the entire pH range, and the other mechanism regulates the pK value of the pH profile of the $E^{\circ\prime}$ value through alteration of the pK_a value of the buried heme 17-propionic acid side chain. The former has been shown to be determined through the Fe−Met bond stability, as previously demonstrated (*16*), and the latter is likely to be executed through alteration of the electrostatic environment around the heme 17-propionic acid side chain (*28*, *32*). As shown in Figure 5, the relationship between the $E^{\circ\prime}$−pH plots of PA and the F7A/V13M/V78I triple mutant was similar to that between the plots of the F34Y/E43Y double mutant and qm. This finding demonstrated that the two mechanisms for the control of the $E^{\circ\prime}$ value in the protein operate independently.

The difference in the $E^{\circ\prime}$ value between PA and the F7A/V13M/V78I triple mutant was ∼70 mV throughout the pH range that was examined, and was identical to that between the F34Y/E43Y double mutant and qm (F7A/V13M/F34Y/E43Y/V78I). These findings indicated that the effects of the F7A, V13M, and V78I mutations on the $E^{\circ\prime}$ value of a protein are independent of the protein which has these amino acid substitutions. According to the X-ray structure of PA (*8*), the mutations examined in our study are located in three spatially separated regions within the framework of the protein structure: region I (F7A and V13M), region II (F34Y

and E43Y), and region III (V78I). Detailed thermodynamic characterization of the protein stability of PA and its mutants demonstrated not only that the mutations in the three regions contribute to the overall protein stability in an additive manner but also that the mutations in regions I and III stabilize the protein structure through both enthalpic and entropic contributions as a result of improved packing of the amino acid side chains in the protein interior, while those in region II enhance the protein stability enthalpically through electrostatic interactions (*13*). These electrochemical data on PA and its mutants are essentially consistent with the conclusions drawn on thermodynamic characterization of the proteins. Thus, this study has successfully provided a molecular basis for quantitative evaluation of the redox function of cyts *c* in terms of their thermodynamic properties.

The characterization of the pH profiles of the $E^{\circ\prime}$ values of PA and the mutants allowed detailed evaluation of the effects of the amino acid substitutions on the ΔG_{RC} and ΔG_{EI} contributions. As demonstrated by the difference in the $E^{\circ\prime}$−pH plots between PA and the F7A/V13M/V78I triple mutant or between the F34Y/E43Y double mutant and qm (Figure 5), the ΔG_{RC} contribution appears to be essentially independent of pH, although the stabilities of the oxidized proteins themselves have been shown to be pH-dependent (*13*). Consequently, the pH profile of the stability of a given protein should be independent of the oxidation state of the heme iron to render the ΔG_{RC} contribution insensitive to pH. On the other hand, the observed pH-dependent $E^{\circ\prime}$ values of the proteins have been attributed predominantly to the ΔG_{EI} contribution arising from the ionization of the buried heme 17-propionic acid side chain in the proteins, as has been demonstrated for wild-type PA (*28*, *32*). These findings provide novel insights into the functional regulation of cyts *c*, which could be utilized for tuning the $E^{\circ\prime}$ values of the proteins by means of protein engineering.

ACKNOWLEDGMENT

The ^{1}H NMR spectra were recorded on a Bruker AVANCE-600 spectrometer at the Chemical Analysis Center, University of Tsukuba.

SUPPORTING INFORMATION AVAILABLE

^{1}H NMR spectra (600 MHz) of the oxidized forms of the proteins [PA and F34Y single, E43Y single, F34Y/E43Y double, F7A/V13M/V78I triple, and F7A/V13M/F34Y/E43Y/V78I quintuple (qm) mutants] in a 90% H_2O/10% ^2H_2O mixture at various pHs, cyclic voltamgram of PA at pH 5.0 and 25 °C, pH profiles of the $E^{\circ\prime}$ values of the proteins, temperature dependence of absorption spectra (630−800 nm) of the proteins, and the pH dependence of the dissociation temperature of the Fe−S coordination bond of the oxidized forms of PA, the F34Y single mutant, and the F7A/V13M/V78I triple mutant. This material is available free of charge via the Internet at http://pubs.acs.org.

REFERENCES

1. Warshel, A., Papazyan, A., and Muegge, I. (1997) Microscopic and semimacroscopic redox calculations: What can and cannot be learned from continuum models, *J. Biol. Inorg. Chem. 2*, 143−152.
2. Gunner, M. R., Alexov, E., Torres, E., and Lipovaca, S. (1997) The importance of the protein in controlling the electrochemistry of heme metalloproteins: Methods of calculation and analysis, *J. Biol. Inorg. Chem. 2*, 126−134.
3. Battistuzzi, G., Bellei, M., Borsari, M., Canters, G. W., de Waal, E., Jeuken, L. J., Ronieri, A., and Sola, M. (2003) Control of metalloprotein reduction potential: Compensation phenomena in the reduction thermodynamics of blue copper proteins, *Biochemistry 42*, 9214−9220.
4. Blouin, C., and Wallace, C. J. A. (2001) Protein matrix and dielectric effect in cytochrome *c*, *J. Biol. Chem. 276*, 28814−28818.
5. Springs, S. L., Bass, S. E., and McLendon, G. L. (2000) Cytochrome b_{562} variants: A library for examining redox potential evolution, *Biochemistry 39*, 6075−6082.
6. Moore, G. R., and Pettigrew, G. W. (1990) *Cytochromes c: Evolutionary, structural, and physicochemical aspects*, Springer-Verlag, Berlin.
7. Scott, R. A., and Mauk, A. G., Eds. (1996) *Cytochrome c*: *A multidisciplinary approach*, University Science Books, Sausalito, CA.
8. Matsuura, Y., Takano, T., and Dickerson, R. E. (1982) Structure of cytochrome c_{551} from *Pseudomonas aeruginosa* refined at 1.6 Å resolution and comparison of the two redox forms, *J. Mol. Biol. 156*, 389−409.
9. Sanbongi, Y., Ishii, M., Igarashi, Y., and Kodama, T. (1989) Amino acid sequence of cytochrome *c*-552 from a thermophilic hydrogen-oxidizing bacterium, *Hydrogenobacter thermophilus*, *J. Bacteriol. 171*, 65−69.
10. Hasegawa, J., Yoshida, T., Yamazaki, T., Sambongi, Y., Yu, Y., Igarashi, Y., Kodama, T., Yamazaki, K., Kyogoku, Y., and Kobayashi, Y. (1998) Solution structure of thermostable cytochrome *c*-552 from *Hydrogenobacter thermophilus* determined by ^{1}H NMR spectroscopy, *Biochemistry 37*, 9641−9649.
11. Hasegawa, J., Shimahara, H., Mizutani, M., Uchiyama, S., Arai, H., Ishii, M., Kobayashi, Y., Ferguson, S. J., Sambongi, Y., and Igarashi, Y. (1999) Stabilization of *Pseudomonas aeruginosa* cytochrome c_{551} by systematic amino acid substitutions based on the structure of thermophilic *Hydrogenobacter thermophilus* cytochrome c_{552}, *J. Biol. Chem. 274*, 37533−37537.
12. Hasegawa, J., Uchiyama, S., Tanimoto, Y., Mizutani, M., Kobayashi, Y., Sambongi, Y., and Igarashi, Y. (2000) Selected mutations in a mesophilic cytochrome *c* confer the stability of a thermophilic counterpart, *J. Biol. Chem. 275*, 37824−37828.
13. Uchiyama, S., Hasegawa, J., Tanimoto, Y., Moriguchi, H., Mizutani, M., Igarashi, Y., Sambongi, Y., and Kobayashi, Y. (2002) Thermodynamic characterization of variants of mesophilic cytochrome *c* and its thermophilic counterpart, *Protein Eng. 15*, 455−461.
14. Sambongi, Y., Uchiyama, S., Kobayashi, Y., Igarashi, Y., and Hasegawa, J. (2002) Cytochrome *c* from a thermophilic bacterium has provided insights into the mechanisms of protein maturation, folding, and stability, *Eur. J. Biochem. 269*, 3355−3361.
15. Terui, N., Tachiiri, N., Matsuo, H., Hasegawa, J., Uchiyama, S., Kobayashi, Y., Igarashi, Y., Sambongi, Y., and Yamamoto, Y. (2003) Relationship between redox function and protein stability of cytochromes *c*, *J. Am. Chem. Soc. 125*, 13650−13651.
16. Yamamoto, Y., Terui, N., Tachiiri, N., Minakawa, K., Matsuo, H., Kameda, T., Hasegawa, J., Sambongi, Y., Uchiyama, S., Kobayashi, Y., and Igarashi, Y. (2002) Influence of amino acid side chain packing on Fe-methionine coordination in thermostable cytochrome *c*, *J. Am. Chem. Soc. 124*, 11574−11575.
17. Moore, G. R., Pettigrew, G. W., and Rogers, N. K. (1986) Factors influencing redox potentials of electron transfer proteins, *Proc. Natl. Acad. Sci. U.S.A. 83*, 4998−4999.
18. Mauk, A. G., and Moore, R. G. (1997) Control of metalloprotein redox potentials: What does site-directed mutagenesis of hemoproteins tell us? *J. Biol. Inorg. Chem. 2*, 119−125.
19. Uchiyama, S., Ohshima, A., Nakamura, S., Hasegawa, J., Terui, N., Takayama, S. J., Yamamoto, Y., Sambongi, Y., and Kobayashi, Y. (2004) Complete thermal-unfolding profiles of oxidized and reduced cytochromes *c*, *J. Am. Chem. Soc. 126*, 14684−14685.
20. Komar-Panicucci, S., Weis, D., Bakker, G., Qiao, T., Sherman, F., and McLendon, G. (1994) Thermodynamics of the equilibrium unfolding of oxidized and reduced *Saccharomyces cerevisiae* iso-1-cytochromes *c*, *Biochemistry 33*, 10556−10560.
21. Ferri, T., Poscia, A., Ascoli, F., and Santucci, R. (1996) Direct electrochemical evidence for an equilibrium intermediate in the guanidine-induced unfolding of cytochrome *c*, *Biochim. Biophys. Acta 1298*, 102−108.

22. Battistuzzi, G., Borsari, M., Sola, M., and Francia, F. (1997) Redox thermodynamics of the native and alkaline forms of eukaryotic and bacterial class I cytochromes *c*, *Biochemistry 36*, 16247−16258.
23. Tezcan, F. A., Winkler, J. R., and Gray, H. B. (1998) Effects of ligation and folding on reduction potentials of heme proteins, *J. Am. Chem. Soc. 120*, 13383−13388.
24. Battistuzzi, G., Borsari, M., and Sola, M. (2001) Medium and temperature effects on the redox chemistry of cytochrome *c*, *Eur. J. Inorg. Chem.*, 2989−3004.
25. Battistuzzi, G., Borsari, M., Ranieri, A., and Sola, M. (2002) Redox thermodynamics of the Fe^{3+}/Fe^{2+} couple in horseradish peroxidase and its cyanide complex, *J. Am. Chem. Soc. 124*, 26−27.
26. Bertini, I., Gori-Savellini, G., and Luchinat, C. (1997) Are unit charges always negligible? *J. Biol. Inorg. Chem. 2*, 114−118.
27. Moore, G. R., Pettigrew, G. W., Pitt, R. C., and Williams, R. J. P. (1980) pH dependence of the redox potential of *Pseudomonas aeruginosa* cytochrome *c*-551, *Biochim. Biophys. Acta 590*, 261−271.
28. Moore, G. R. (1983) Control of redox properties of cytochrome *c* by special electrostatic interactions, *FEBS Lett. 161*, 171−175.
29. Churg, A. K., and Warshel, A. (1986) Control of the redox potential of cytochrome and microscopic dielectric effects in proteins, *Biochemistry 25*, 1675−1681.
30. Davies, A. M., Guillemette, J. G., Smith, M., Greenwood, C., Thurgood, A. G. P., Mauk, A. G., and Moore, G. R. (1993) Redesign of the interior hydrophilic region of mitochondrial cytochrome *c* by site-directed mutagenesis, *Biochemistry 32*, 5431−5435.
31. Cutler, R. L., Davies, A. M., Creighton, S., Warshel, A., Moore, G. R., Smith, M., and Mauk, A. G. (1989) Role of arginine-38 in regulation of the cytochrome *c* oxidation−reduction equilibrium, *Biochemistry 28*, 3188−3197.
32. Leitch, F. A., Moore, G. R., and Pettigrew, G. W. (1984) Structural basis for the variation of pH-dependent redox potentials of *Pseudomonas* cytochromes *c-551*, *Biochemistry 23*, 1831−1838.
33. Cutruzzolà, F., Ciabatti, I., Rolli, G., Falcinelli, S., Arese, M., Ranghino, G., Anselmino, A., Zennaro, E., and Silvestrini, M. C. (1997) Expression and characterization of *Pseudomonas aeruginosa* cytochrome *c*-551 and two site-directed mutants: Role of tryptophan 56 in the modulation of redox properties, *Biochem. J. 322*, 35−42.
34. Takano, T., and Dickerson, R. E. (1981) Conformation change of cytochrome *c*: I. Ferrocytochrome *c* structure refined at 1.5 Å resolution, *J. Mol. Biol. 153*, 79−94.
35. Takano, T., and Dickerson, R. E. (1981) Conformation change of cytochrome *c*: II. Ferricytochrome *c* refinement at 1.8 Å and comparison with the ferrocytochrome structure, *J. Mol. Biol. 153*, 95−115.
36. Berghuis, A. M., and Brayer, G. D. (1992) Oxidation state-dependent conformational changes in cytochrome *c*, *J. Mol. Biol. 223*, 959−976.
37. Banci, L., Bertini, I., Huber, J. G., Spyroulias, G. A., and Turano, P. (1999) Solution structure of reduced horse heart cytochrome *c*, *J. Biol. Inorg. Chem. 4*, 21−31.
38. Taniguchi, I., Iseki, M., Eto, T., Toyosawa, H., Yamaguchi, H., and Yasukouchi, K. (1984) The effect of pH on the temperature dependence of the redox potential of horse heart cytochrome *c* at a bis(4-pyridyl)disulfide-modified gold electrode, *Bioelectrochem. Bioenerg. 13*, 373−383.
39. Ueyama, S., Isoda, S., Hatanaka, H., and Shibano, Y. (1996) Macroscopically rapid electron transfer of cytochrome c_{522} with high thermostability at bare and surface-modified gold electrodes, *J. Electroanal. Chem. 401*, 227−230.
40. Cuttruzzolá, F., Arese, M., Ranghino, G., van Pouderroyen, G., Canters, G., and Brunori, M. (2002) *Pseudomonas aeruginosa* cytochrome c_{551}: Probing the role of the hydrophobic patch in electron transfer, *J. Inorg. Biochem. 88*, 353−361.
41. La Mar, G. N., Satterlee, J. D., and de Ropp, J. S. (2000) Nuclear magnetic resonance of hemoproteins, in *The porphyrin handbook* (Kadish, K., Smith, K. M., and Guilard, R., Eds.) pp 185−298, Academic Press, New York.
42. Bertini, I., and Luchinat, C. (1986) *NMR of Paramagnetic molecules in biological systems*, pp 19−46, The Benjamin/Cummings Publishing Co., Menlo Park, CA.
43. Yamamoto, Y. (1998) NMR study of active sites in paramagnetic hemoproteins, *Annu. Rep. NMR Spectrosc. 36*, 1−77.
44. Dutton, P. L. (1978) Redox potentiometry: Determination of midpoint potentials of oxidation−reduction components of biological electron-transfer systems, *Methods Enzymol. 54*, 411−434.
45. Tachiiri, N., Hemmi, H., Takayama, S. J., Mita, H., Hasegawa, J., Sambongi, Y., and Yamamoto, Y. (2004) Effects of axial methionine coordination on the in-plane asymmetry of the heme electronic structure of cytochrome*c*, *J. Biol. Inorg. Chem. 9*, 733−742.
46. Simonson, T., Carlsson, J., and Case, D. A. (2004) Proton binding to proteins: pK_a calculations with explicit and implicit solvent models, *J. Am. Chem. Soc. 126*, 4167−4180.

BI047498S